CHAPTER – 3

METHODS

The present study area, the Katrol Hill Fault (KHF) zone is a largely rocky landscape coupled with a lack of good complete sections due to the above-mentioned complexities encountered in the study area, except the Khari river section which shows clear offsetting of the Quaternary sediments overlying the Mesozoic rocks (Patidar et al., 2008). This meant that the tracing of surface faulting along KHF could not be done using routine field studies alone. Thus, the approach and the methodology applied in the present study were largely governed by the area-specific conditions. In view of this, a multipronged strategy that used field mapping, geomorphological studies, shallow geophysical studies using Ground Penetrating Radar (GPR), microscopic studies (petrography and SEM) and calculation of moment magnitude (M_w) of the events using available empirical relationships was followed in order to describe the seismogenic potential of the KHF. The flowchart given in Figure 3.1 summarises the approach and methods adopted in the present study. The following description gives details of the various methods used in the present study.

FIELD MAPPING

The field investigation includes close examination of the surface outcrops and lithological contacts present in the study area. Lateral as well as vertical relationships of the lithological units belonging to different formations and their extent, mainly the Quaternary deposits, have been critically observed. Field study was carried out along the Katrol Hill Fault (KHF) zone. To understand the deformation activity of KHF over the Quaternary sediments, the field study was started from the well explored and dated site of Khari river cliff section (23º11'36.43"N, 69º35'22.49"E) first reported by Patidar et al., (2008). An attempt has been made to observe the effects of the surface rupturing seismic activity along the KHF.

In order to observe the geomorphic effects of surface faulting in the KHF zone, the field investigations comprised traverses along the Gunawari and Gangeshwar river basins and KHF in the study area to document present-day landscape characteristics and anomalous geomorphic features. Sampling of Late Quaternary miliolite deposits found very near or exactly on the fault trace was carried out for microscopic analyses. For comparison purposes, samples were also collected from the miliolite deposits lying away from the fault zone to examine the difference in the microscopic properties of the rocks.

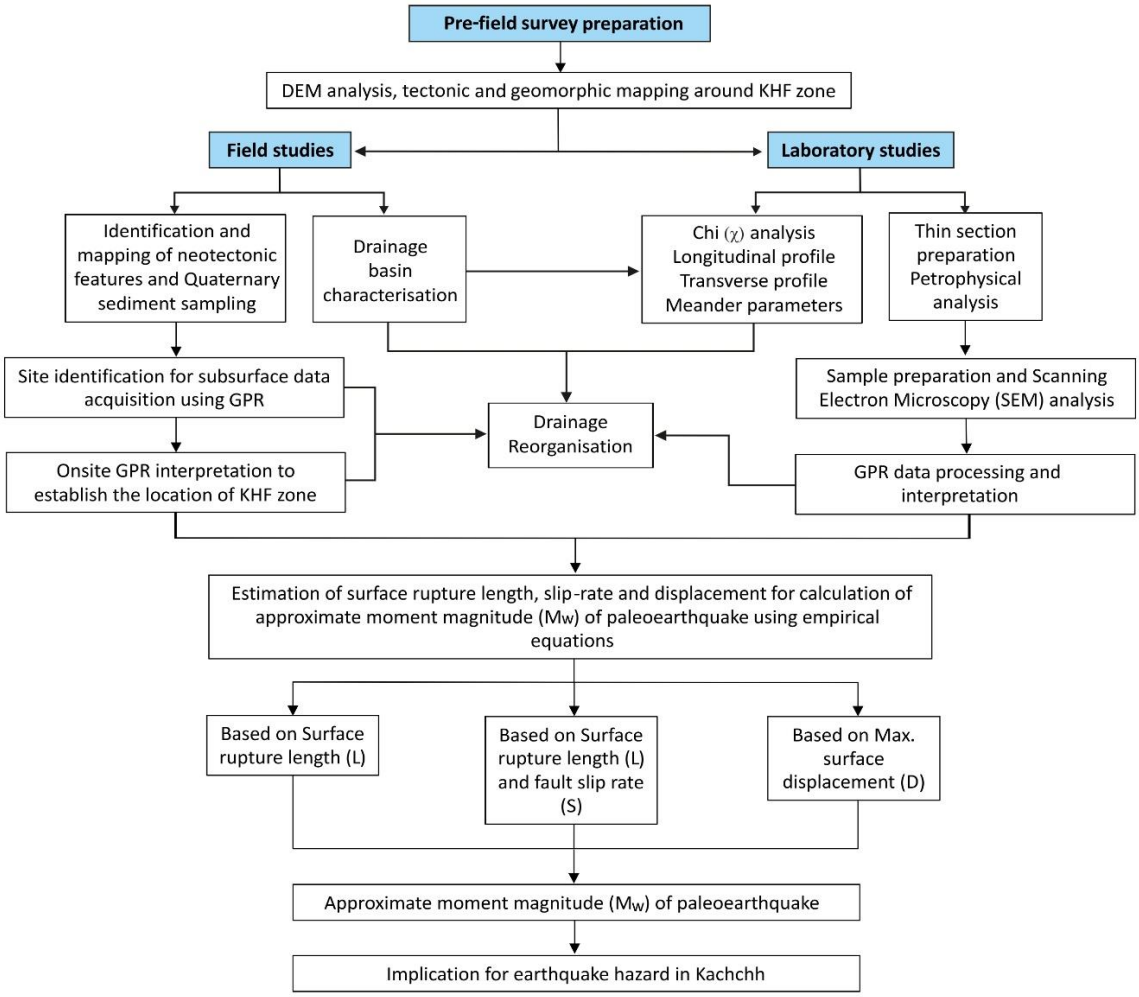

Figure 3.1 Flowchart summarizing the approach and methods adopted in the present study.

GROUND PENETRATING RADAR (GPR)

The shallow subsurface proves to be the most important geological layer in the Earth for humans as this layer contains many of the Earth's natural resources (e.g., building materials, placer deposits, aquifers, soils, etc.) and also acts as a sink for human waste (e.g., landfill sites) (Neal, 2004). In addition, the study of unconsolidated sediment accumulations at or near the surface tell us much about Earth's history and the behaviour of its dynamic landforms which have assisted in the fields of managing the environment, such as prediction of natural disasters and exploration for more remote natural resources such as oil and gas. The Ground Penetrating Radar (GPR or ground-probing radar, surface penetrating radar, subsurface radar, georadar or impulse radar) is a non-invasive geophysical technique that detects electrical discontinuities in the shallow subsurface (< 50 m) and has proved to be a robust technique in exploring the shallow subsurface nature of the Earth's crust (Neal, 2004). The electrical discontinuities in the shallow subsurface (typically < 50 m) are detected by the GPR through generation, transmission, propagation, reflection and reception of discrete

high-frequency pulses of electromagnetic energy in the megahertz (MHz = 106 Hz, 1 Hz = 1 cycle/s) frequency range (Neal, 2004).

The present study attempts to map the lateral extent of the paleo-surface rupture along KHF, which is evident in the Khari river section and a couple of other locations (Patidar et al, 2007; 2008; 2019). However, the continuity of the rupture could not be established by surface mapping alone done using field studies, owing to the discontinuous Quaternary sediment cover attributed to the erosional topography of the arid region experienced by the KHF zone and the overall Kachchh region. To bridge this information gap, high-resolution geophysical technique, Ground Penetrating Radar (GPR), was used to investigate the shallow sub-surface nature of KHF and evidence of Quaternary sediment deformation. SIR-20 GPR system (GSSI, USA) along with 200 MHz monostatic antenna was used to obtain shallow subsurface profiles from multiple locations across the KHF zone. The 200 MHz antenna frequency provides an 8-9 m optimum penetration, which was sufficient for the thin sediment cover in the study area. A detailed description of the fundamentals and working principles of GPR can be found in (Davis and Annan, 1989; Smith and Jol, 1995; Maurya et al., 2005; Patidar et al., 2006). GPR data in the form of 2D profiles were acquired along transects in the buried paleo-valley, wind gap and Late Quaternary deposits overlying the Katrol Hill Fault (KHF) for a comprehensive study of geomorphic effects of surface faulting along the KHF.

As is the common practice, multiple profiles were acquired across the direction of fault strike at sites selected after the study of satellite images, DEM interpretations, field observations and careful geomorphic mapping. Finally, a subset of the profiles was selected and subjected to post-survey processing using RADAN software.

GPR data acquisition and data processing

The geo-physical GPR method, its data collecting and processing steps are discussed as follows. The GPR instrument consists of an antenna (transmitter-receiver pair) and a recorder as shown in Figure 3.2.

The Transmitter transfers high frequency wave in to the layers of the Earth and the receiver antenna receives the reflected waves from the different layers constituting the Earth's subsurface (Aksu et al., 2017). The propagation of signals in the layers of the Earth depends on their magnetic and electrical properties such that, some signals are reflected from the subsurface while, some are transmitted. The recorder records the reflected and diffracted signals along the GPR profile by a desired specified interval. The penetration depth, value of diffraction and absorption of the signal depends upon the chosen frequency value such

as, when the frequency decreases, the penetration depth increases and vertical resolution decreases and vice versa (Davis and Annan, 1989; Fisher et al., 1992). The collected data are processed by various filtering methods for interpretation.

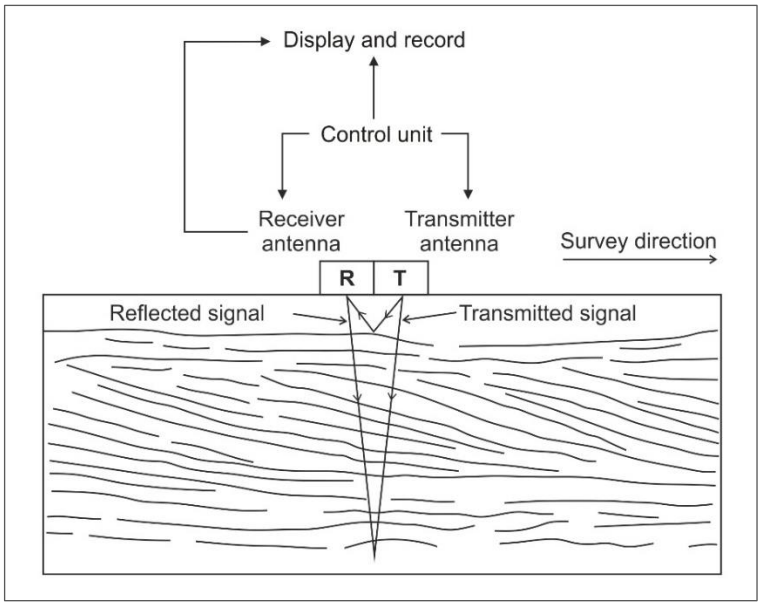

Figure 3.2 GPR data acquisition system showing the main components of GPR system and configuration of subsurface reflectors. Modified from Neal (2004).

The post-survey processing of GPR data was performed using RADAN (v.7) software by GSSI Inc. The raw GPR profiles acquired from rugged topographic surfaces require filtering of noise/ unwanted signals, which substantially mask the useful reflections (Aksu et al., 2017). The GPR data acquired in the present study was processed with a view to improving the interpretability of subsurface stratigraphic features and deformational structures. In general, most of the GPR profiles showed less noise in the shallow section, but a few GPR profiles showed ringing noise at deeper intervals, which was removed by background removal filter (Kim et al., 2007). The following are the necessary data processing steps: *(i)* muting of surface waves – at the top of the radargram, the horizontal strong amplitude of air wave and ground wave are muted. This led to keep the topmost scan of the radargram in close approximation with the ground surface. Topographic correction is applied. *(ii)* Background removal – the horizontal high pass background removal filter is applied to eliminate the high-amplitude constant horizontal banding prevalent at the top of the radargrams (Kim et al., 2007). The continuous, long reflections which are persistent in the radargrams recorded across the paleo-valley are also removed by using high pass background removal filter. *(iii)* Band-pass filtering – the desired signals are further enhanced by eliminating the out of frequency noise. The vertical low- and high-pass FIR filter of 400 and 70 MHz cut-off frequency, respectively, is applied. It removes the frequencies above

and below the established threshold to a great extent and improved the overall visibility of the true reflections. The horizontal low-pass smoothing IIR filter of 3-5 scans is then applied to reduce the snow-like noise at depth and to remove the sharp vertical low-frequency bands. *(iv)* Range gain – The linear range gain is applied to artificially increase the amplitudes of radar signals, to offset the attenuation caused during processing described earlier and to improve the visibility of reflectors (Davis and Annan, 1989; Peters et al., 1994). *(v)* Semblance analysis – the average Electro-Magnetic (EM) waves velocity of 0.13 m ns^{-1} determined through acquired CMP gather is used for time-depth conversion. *(vi)* Surface normalization – the vertical scale of the processed radargram is adjusted to correct for the topographic changes.

MICROSCOPIC ANALYSES

Several microscopic methods have been proposed for seismological investigation of faults where basement rocks are exposed at the surface without the presence of macrostructures and sedimentary covers by workers such as Kanaori et al. (1980), Ikeya et al. (1982), Kanaori (1983), Kralik et al. (1987), Menzies and Taylor (2003) and Zwingmann and Mancktelow (2004). The purpose of such microscopic analyses is to confirm that deformation due to neotectonic faulting events has reached up to the surface in the Quaternary deposits. No study has been attempted in the seismically active region of Kachchh, which concerns with the microscopic characterization of recent deposits that have also experienced neotectonic faulting. In the present study, the microscopic characterization of the Late Quaternary miliolite deposits has been done using the optical microscope and the Scanning Electron Microscope (SEM).

Petrography

Petrographic analysis of thin sections by transmitted light microscopy is one of the principal methods for rock characterization and classification. The accurate determination of the features that result from petrogenetic processes is central in the fields of petrology, volcanology or tectonics (Jerram et al., 2003; Higgins, 2006; Trullenque et al., 2006; Keulen et al., 2007; Piochi et al., 2008). Van der Meer and Menzies (2011) considered micromorphological analyses (thin-section analysis) as a valuable tool to determine the impact of seismic activity on sediments and in areas where known seismic activity has apparently long ceased to be regarded as significant but may constitute considerable future environmental risks. Jeong and Cheong (2005) also emphasized the use of mineralogical and micromorphological approaches in environments where sediments face rapid

degradation and lack datable materials useful for paleo-seismological interpretations. The KHF is one such fault in the seismically active Kachchh basin where the last event of surface faulting was recorded at ~3 ka BP (Kundu et al., 2010) and no activity has been reported along KHF since. Due to insufficient macroscopic or field evidences of surface faulting in Quaternary sediments along the KHF zone, samples were collected during field studies for thin-section analysis to examine the grain-scale effects of deformation in Quaternary deposits.

A rock chip was sliced off from each sample for petrographic analysis using optical microscope. One surface of the rock chip was ground to fine smoothness and was mounted on to the glass slide with help of Araldite (resin and hardener) and then clamped to prevent development of air bubbles. After overnight cooling and curing, the thin sections were prepared using an automated thin section preparation machine. These thin sections were later placed under Leica Petrological Microscope attached with the microphotography system for taking photographs of the texture and mineral characteristics of samples.

Scanning Electron Microscopy (SEM)

With the introduction of the electron microscope in the early 20th century, studies regarding the analysis of quartz grains from various environments had substantially improved, which facilitated micrometre sized observation of the textures on quartz grains (Bull, 1981). Later with the technical advancements, the scanning electron microscope (SEM) was introduced in the 1960's which permitted the grains to be observed at higher resolution. The scanning electron microscope (SEM) is considered to be one of the most versatile instruments for the examination and analysis of the surface microstructure morphologies of various materials (Zhou et al., 2006; Vos et al., 2014). It utilizes a focused electron beam to scan across the surface of the specimen systematically, producing large numbers of signals, the detailed working of the microscope is discussed in the 'SEM configuration' section.

There have been numerous SEM studies about the microtextures on the quartz grain surfaces describing how they have proven useful for determining the transportational and depositional history of quartz sand grains belonging to a variety of environments such as glacial, fluvial, glaciolacustrine and aeolian (Mahaney, 1995; Mahaney et al., 2008; Vos et al., 2014). The use of quartz grain surface textures for sites affected by faulting has also been demonstrated (Kanaori et al., 1980a; 1985; Kanaori, 1983; Mizoguchi and Ueta, 2013; Niwa et al., 2016). Mahaney et al. (2004) reported deformational microtextures and microstructures. However, equivalent studies on detrital quartz grains from recent

Quaternary deposits which have undergone several episodes of neotectonic faulting are limited. In the present study, SEM on the quartz grain surfaces has been performed to observe the effects of surface faulting (neotectonic deformation) on samples collected from the Late Quaternary miliolite deposits found along and away from the KHF zone. The presence of microtextures on quartz grain surfaces which are subjected to breakage and fracturing due to neotectonic faulting along KHF zone are observed. Further, the observed microtextures are correlated with those found in other tectonically active faults of the world, in an attempt to establish lateral continuity of surface rupture between the sites recording Quaternary deformation located in the KHF zone. Quartz is the most commonly used mineral for SEM study, as it is particularly resistant to mechanical breakdown during erosion of rocks and exhibits extreme ability to resist chemical attack by atmospheric agents, soil acids and percolating waters. Such resistant nature of quartz enables it to be used to reconstruct the various agencies that have acted upon the sand grain in the geological past (Vos et al., 2014).

SEM sample preparation

For separation of quartz grains, 50 g of each sample was treated with 36% HCl for 24 hours to remove the carbonate covering from the surface of quartz grains. After this, the sediments were rinsed with deionized water until the decanted water was clear and turned out to be neutral on a pH strip. The sediments were then carefully collected on a filter paper and then oven-dried for one and a half hours at 60°C temperature. No further treatment was done as impurities like iron oxide and other organic debris materials were not observed. After drying the sample, about 35-40 grains were selected at random from each sample for SEM analysis (Figure 3.3).

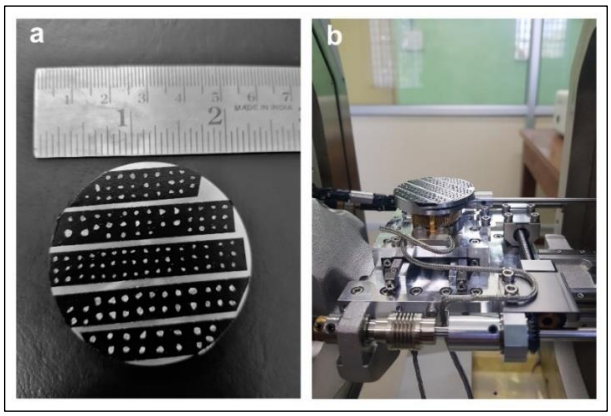

Figure 3.3 a. Quartz grains mounted on SEM stage. **b.** SEM stage in the column chamber. Photographs taken in SEM lab at Department of Geology, The MS University of Baroda.

The grains were then carefully mounted on the SEM stage covered with double sticky carbon tape. The grains were arranged into rows as shown in Figure 3.3a to avoid confusion during SEM viewing. The specimens were then subjected to gold coating for better surface conduction before conducting SEM analysis. The stage was then placed in the column chamber as shown in Figure 3.3b for the quartz grains to be analysed.

SEM configuration

The scanning electron microscope (SEM) comprises of two major components - the column and the cabinet as shown in Figure 3.4. The column is the extent that electrons traverse from their emission until they reach the sample, where they encounter the installed detectors that capture the scattered signals resulting from the interaction between the electrons and the sample. The detectors act as energy transducers that convert the signal received into an electrical signal, which is then sent to the control cabinet. The control cabinet consist of electronic systems that quantify the electrical signals sent by the detectors and transform them into analysable information such as images and graphs (Pereira-da-Silva and Ferri, 2017).

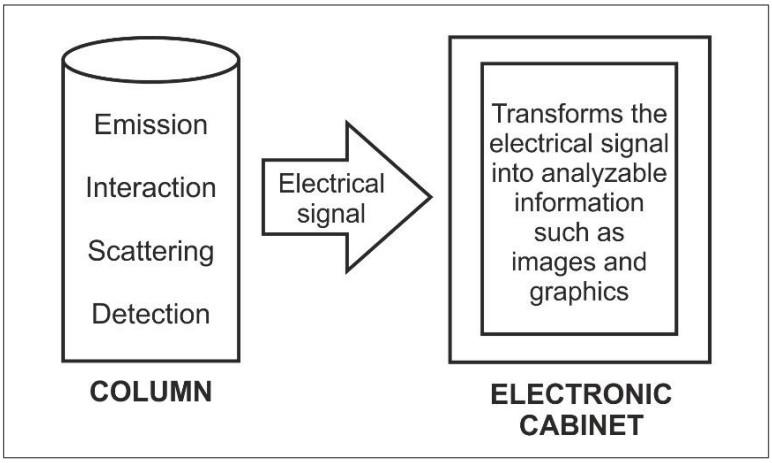

Figure 3.4 An electron column showing the elements relating to the signals from their emission till they are captured. The processing of signals takes place in the cabinet. Modified from Pereira-da-Silva and Ferri (2017).

A column structure of a conventional SEM is shown in Figure 3.5. The electron gun which lies on the top of the column, produces and accelerates the electrons to an energy level of 0.1–30 keV. As the diameter of electron beam which is produced by hairpin tungsten gun is too large to form a high-resolution image, the electromagnetic lenses and apertures focus and define the electron beam to form a small focused electron spot on the specimen. This process is required in order to demagnify the size of the electron source (~50 μm for a tungsten filament) down to the final required spot size (1–100 nm). An ultra-high vacuum

system is crucial for SEMs in order to avoid the scattering on the electron beam and the contamination of the electron guns and other components. The real-time observation and image recording of the specimen surface is provided by the specimen stage, electron beam scanning coils, signal detection and processing system.

The secondary electron (SE) emission signal is the most widely used signal produced by the interaction of the primary electron beam with the specimen (Zhou et al., 2006). The secondary electrons, which are the loosely bound electrons, are emitted when the primary beam strikes the sample surface causing the ionization of specimen atoms. These electrons can only escape from a region within a few nanometres of the material surface due to their low energy of around 3–5 eV. Thus, the secondary electrons are used principally for topographic contrast in the SEM i.e., for the visualization of surface texture and roughness, as they precisely mark the position of the beam and give topographic information with good resolution. The topographical image is dependent on the number of the secondary electrons that actually reach the detector. A resolution of 10 nm or better can be obtained for surface structures from a secondary electron signal.

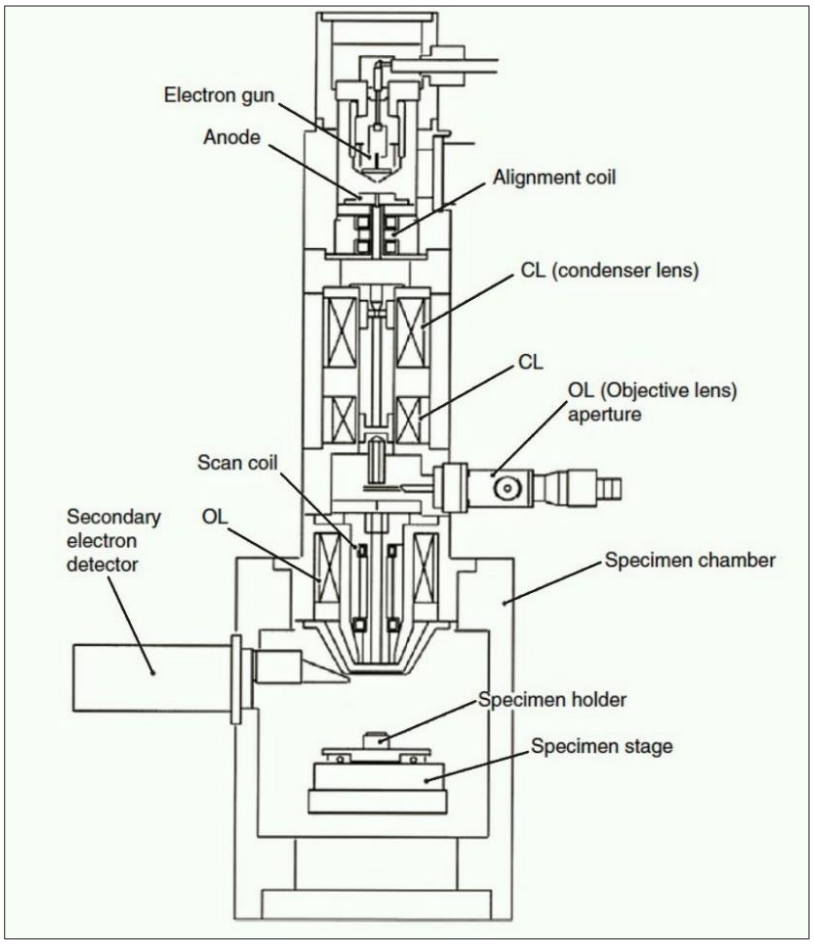

Figure 3.5 Schematic figure of a conventional scanning electron microscope. Modified from Zhou et al. (2006).

A Hitachi SU1510 Scanning Electron Microscope at the Department of Geology, The M. S. University of Baroda in Vadodara (India) was used for the present study. The electron source was pre-centered cartridge type tungsten hairpin filament which generates and accelerates electrons at a constant emission current of 100 μA and varying voltages of 15 to 30 kV and a secondary electron image was obtained in high vacuum mode. In order to be able to observe grain outlines and to identify the μm-scale features on the grain surface, the magnification was varied from 100× up to 1000×. The image was captured by a high-definition camera (5120x3840 pixels). The magnification, scale and working distance are specified in SEM image for better observation.

CALCULATION OF MOMENT MAGNITUDE (M_w)

Various workers such as Anderson et al. (1996), Leonard (2014), Wyss (1979), Schwartz et al. (1984), Wells and Coppersmith (1994) and Thingbaijam et al. (2017) formulated scaling relationships which directly correlate the magnitude of the earthquake with different fault parameters such as fault surface and sub-surface rupture length, fault rupture area, displacement, seismic moment and slip-rate. However, in the present study, the displacement and slip rates of the three surface faulting events that occurred during Late Quaternary as observed in the Khari river section, in addition to mapping the surface rupture length using the above-mentioned techniques of GPR, optical microscopy and SEM were estimated. Thus, by making use of these three parameters of surface faulting along KHF viz. surface rupture length, displacement and slip rate, the magnitude (M_w) of faulting was estimated by the equations given by Slemmons (1982)**,** Wells and Coppersmith (1994) and Anderson et al. (1996) which are derived after careful compilation of worldwide historical earthquake events.

For estimating the magnitude from the length of surface rupture, the equation given by Slemmons (1982) and Wells and Coppersmith (1994) was used. According to Slemmons (1982), which correlates the surface rupture length of faulting to the magnitude as,

$$M_s = 2.021 + 1.142 \log L \quad (1)$$

where, L is the rupture length in meters.

Whereas, the relationship between surface rupture length of faulting and moment magnitude (M_w) given by Wells and Coppersmith (1994) is,

$$M = a + b * \log (SRL) \quad (2)$$

where, a and b are constants with values 5.08 and 1.16 respectively and SRL is the surface rupture length in kilometre.

Slemmons (1982) gave the following relationship using displacement to estimate the magnitude of an earthquake as,

$$M_s = 6.793 + 1.306 \log D \quad (3)$$

where, D is maximum surface displacement in meters.

Wells and Coppersmith (1994) obtained the equation correlating displacement and moment magnitude (M_w) as,

$$M_w = a + b * \log (MD) \quad (4)$$

where, MD is maximum displacement, a and b are regression coefficients with 6.69 and 0.74 values respectively.

Anderson et al. (1996) formulated a regression equation correlating surface rupture length (L) and fault slip rate (S) with a moment magnitude (M_w) and deduced the equation as,

$$M_w = A + B \log L + C \log S \quad (5)$$

where, A, B and C in the equation are constants determined by standard least squares regression method possessing the values of 5.12 $\pm$0.12, 1.16 $\pm$0.07 and 0.20 $\pm$0.04 respectively and believed that this equation offered more accurate predictions than those exclusively based on fault rupture length (L) as proposed by Well and Coppersmith (1994) (Eq. 2).

All the above-mentioned equations were utilized in the present study, to estimate magnitude of surface faulting which took place along the KHF during the Late Quaternary.

MORPHOMETRIC MEANDER PARAMETERS

River meander parameters are important indicators of channel morphology at river basin scales (Bathurst et al., 1979; Nanson, 2010; Hooke, 2013; Yousefi et al., 2016). To supplement the field observations of present-day channel characteristics, morphometric parameters such as river width (W), radius of curvature (R), axis length (A), meander neck length (L), water flow length (S), sinuosity (C) of the stream (Figure 3.6) and width-to-depth ratio for Gunawari and Gangeshwar rivers were calculated as per the methods described by Hooke (2013) and Yousefi et al. (2016).

W is the mean cross section of the meander loops, R is the maximum internal loop in meanders, A is the longest distance between meander neck and internal arc, L is the smallest distance between two meander bends and S is the water length between two meander heads (Yousefi et al., 2016). The sinuosity (C) is obtained by dividing the water flow length (S) with meander neck length (L) i.e., C = S/L (Hooke, 1984; Yousefi et al.,

2016). The width-to-depth ratio was obtained by dividing channel width (W) by mean depth (D) of the channel at the same place (Gaudet and Roy, 1995).

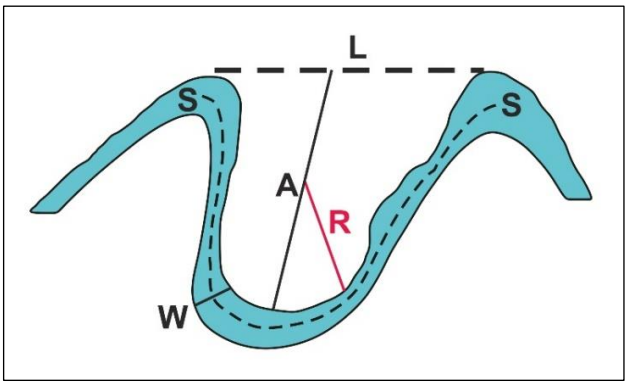

Figure 3.6 Morphometric meander parameters: axis length (A), meander neck length (L), river width (W), radius curvature (R), water flow length (S). Modified from Yousefi et al. (2016).

For estimating these parameters, the present-day Gunawari river channel was digitized and 25 reaches were identified based on visual and spatial changes affecting the meander loops. Basic data required for calculating the parameters were extracted from Survey of India (SOI) topographical maps on 1:50,000 scale, Q-GIS and Google Earth.

CHI (χ) ANALYSIS

The Earth's surface topography evolves over time (Davis, 1899) and provides a basis for reconstructing past tectonic (Pritchard et al., 2009; Kirby and Whipple, 2012) and climatic processes (Tucker and Slingerland, 1997; Hancock and Anderson, 2002); as landforms are the product of the interaction between tectonic and denudational processes. Thus, the geomorphic characterization of any region, based on tectonic and geologic formations is complicated, as the natural processes involved are interrelated and dynamic in nature (Guha and Patel, 2017). The examination of tectonic framework has already been done using well-defined indices (Burbank and Anderson, 2011), presuming uniformity in rock strength (geology) and climatic characteristics (Kale and Shejwalkar, 2008). However, when considering large spatial scales and regions with heterogeneous lithological characteristics, the identification of tectonic indications become difficult due to generalization of the assumptions. Most landscapes comprise of river channels which are dynamic in nature due to their erosional and transportational processes but remain in long-term equilibrium with their bounding river channels (Montgomery and Dietrich, 1988) that exhibit a tendency to get preserved once established, so they incorporate noteworthy information about the past and present tectonic regime (Seeber and Gornitz, 1983; Oberlander, 1985; Gupta, 1997; Twidale, 2004; Yanites and Tucker, 2010; Castelltort et al.,

2012). The patterns of river channels in tectonically active regions may contain important signals for understanding fault movement and its interaction with stream development (Jackson et al., 1996; Burbank and Anderson, 2011).

For this reason, an attempt has been made to identify the geomorphic effects of surface faulting in the Gunawari and Gangeshwar river basins by using the Chi (χ) analysis. The anomalous geomorphic setting and drainage characteristics of the present day Gunawari and Gangeshwar rivers provide clues for the tectonically controlled drainage rearrangement in the recent geologic past. Chi (χ) analysis of the Gunawari River basin and Gangeshwar River basin was carried out, as the parameter χ characterizes the river network topology and geometry and determines how tectonic forcing gives rise to varying topography throughout a river basin (Willett et al., 2018).

It is apparent from the linear form of the equation mentioned below, that χ serves as a metric for the steady-state elevation of a channel at location *x*. Thus, in a region that experiences constant tectonic forcing and displays homogeneous physical properties, a difference in χ across a drainage divide (Figure 3.7a) suggests disequilibrium and apparently, the motion of the divide towards the direction of larger χ to attain equilibrium (Figure 3.7b, c). Therefore, mapping χ throughout a channel network and comparing its values across drainage divides provides a picture of the dynamic reshaping of drainage basins.

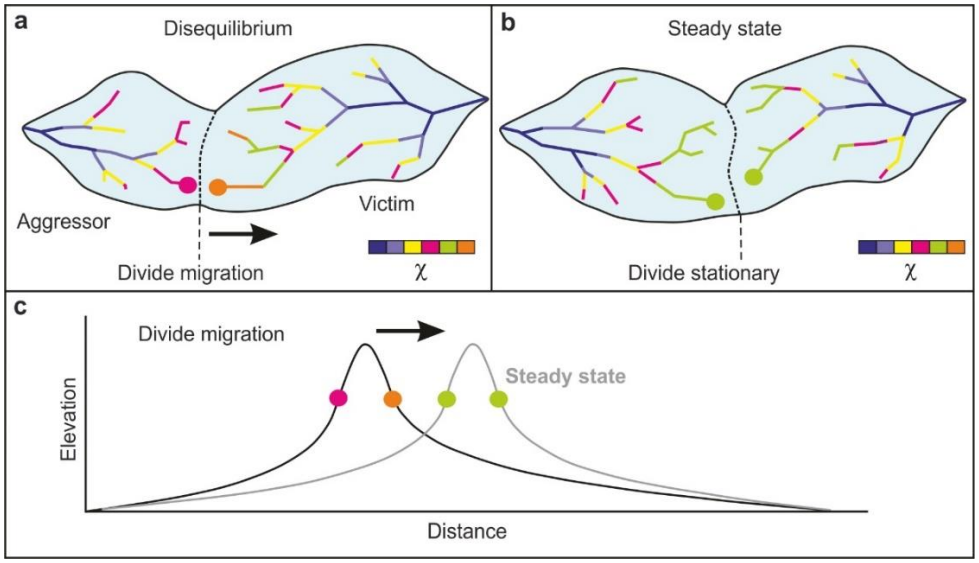

Figure 3.7 Two river basins separated by a common drainage divide. **a.** The existence of two channels in the state of disequilibrium. **b.** Evolution of both the channels from a state of disequilibrium to steady state by experiencing changes in the size and shape. The aggressor basin (towards left) shows lower steady-state elevation at the source, which consequently shifts the position of drainage divide towards the victim basin (right side). **c.** Evolution of the elevation of two channels meeting at the shared divide with respect to distance along the channel. Modified from Willett et al. (2018).

The algorithm and methodology developed by Mudd et al. (2014) is used to carry out the analysis. Spatial distribution of the Chi (χ) parameter from 90 m resolution SRTM DEM of the Gunawari River basin, as a theoretical proxy for steady-state elevation (Perron and Royden, 2013; Willett et al., 2018) was calculated using the Chi (χ) plot equation, which is an integral function of drainage area along the channel network from base level (*xb*) to location *x* (Perron and Royden, 2013; Mudd et al., 2014; 2018), scaled to an arbitrary drainage area A_0 such that:

$$\chi = \int_{xb}^{x} \left(\frac{A_0}{A(x')}\right)^{\frac{m}{n}} dx' \quad (6)$$

where, x' is the variable of integration and m and n are empirical, non-integer constants. The integral method uses elevation as the dependent variable instead of slope and the spatial integral of drainage area as the independent variable and provides an estimation of the steady-state elevation for a given point on a channel. The Chi (χ) map was prepared for both basins; while, Chi (χ) plot (Perron and Royden, 2013) was generated for the main stream of Gunawari River and its tributaries mainly to characterize the present-day drainage of the study area. Chi (χ) map and plot was produced using the QGIS and LSDTopotoolbox channel analysis tool developed by the Land Surface Dynamics Group at the University of Edinburgh, UK (Mudd et al., 2018).

The composite approach to delineate the process of drainage reorganization involved the use of topographic maps, available satellite and SRTM data, Digital Elevation Models (DEMs); detailed field investigations; shallow subsurface geophysical surveys with Ground Penetrating Radar (GPR) and Chi (χ) analysis. The aforesaid methods were supplemented with geomorphic cross sections, longitudinal river profiles and evaluation of morphometric meander parameters for both Gunawari and Gangeshwar rivers.